ADVANCED FUNCTIONAL MATERIALS
www.afm-journal.de

Plasmonic Heterostructure TiO_2-MCs/WO_{3-x}-NWs with Continuous Photoelectron Injection Boosting Hot Electron for Methane Generation

Zaizhu Lou, Peng Zhang, Juan Li, Xianguang Yang, Baibiao Huang,* and Baojun Li**

Nonmetallic plasmonic heterostructure TiO_2-mesocrystals/WO_{3-x}-nanowires (TiO_2-MCs/WO_{3-x}-NWs) are constructed by coupling mesoporous crystal TiO_2 and plasmonic WO_{3-x} through a solvothermal procedure. The continuous photoelectron injection from TiO_2 stabilizes the free carrier density and leads to strong surface plasmon resonance (SPR) of WO_{3-x}, resulting in strong light absorption in the visible and near-infrared region. Photocatalytic hydrogen generation of TiO_2-MCs/WO_{3-x}-NWs is attributed to plasmonic hot electrons excited on WO_{3-x}-NWs under visible light irradiation. However, utilization of injected photoelectrons on WO_{3-x}-NWs has low efficiency for hydrogen generation and a co-catalyst (Pt) is necessary. TiO_2-MCs/WO_{3-x}-NWs are used as co-catalyst free plasmonic photocatalysts for CO_2 reduction, which exhibit much higher activity (16.3 μmol g^{-1} h^{-1}) and selectivity (83%) than TiO_2-MCs (3.5 μmol g^{-1} h^{-1}, 42%) and WO_{3-x}-NWs (8.0 μmol g^{-1} h^{-1}, 64%) for methane generation under UV–vis light irradiation. A photoluminescence study demonstrates the photoelectron injection from TiO_2 to WO_{3-x}, and the nonmetallic SPR of WO_{3-x} plays a great role in the highly selective methane generation during CO_2 photoreduction.

1. Introduction

Plasmonic photocatalyst coupling noble metal nanoparticle (NPs) and semiconductors have been applied in various fields including water splitting,[1–3] environmental treatment,[4,5] and artificial photosynthesis.[6–11] Surface plasmon resonance (SPR) is unique optical property which occurs on rare noble metals (Au, Ag, and Cu) under light irradiation; however, the low-reserve and high-cost noble metals restrict their practical utilization in plasmonic photocatalysis. Recently, some low-cost nonmetallic materials (metal oxides/sulfides) exhibiting SPR phenomenon attracted attentions as potential substitutes of plasmonic noble metals.[12,13] The free carriers density on metal oxides/sulfides can be improved through heavy-doping, similarly with SPR of noble metals, the free carriers oscillate with incident light leading to strong SPR.[14] However, most doped plasmonic NPs exhibited SPR absorption in long wavelength region (>1500) resulting in low energy hot carriers for catalysis.[15] Among various nonmetallic plasmonic NPs, self-doping semiconductors such as WO_{3-x},[16–18] MoO_{3-x}[19,20] and $Cu_{2-x}S$[21,22] are much attractive for their facile synthesis and strong SPR absorption in visible–near-infrared (NIR) region, which have been applied to promote catalysis and cancer therapy by plasmonic thermal effect and sensitization.[23–27] Recently, Cheng et al. reported nonmetallic plasmonic MoO_{3-x} exhibiting plasmon-enhanced hydrogen generation from ammonia borane.[28] While, in strictly, hydrogen generation from ammonia decomposition do not give direct evidence to show the energy transfer from solar light to chemicals. Then, Zhang et al. reported photocatalytic hydrogen generation by plasmonic hot electrons of heterostructural $W_{18}O_{49}$/g-C_3N_4 under visible–NIR light irradiation.[29,30] Therefore, nonmetallic plasmonic NPs are promising SPR materials for photocatalysis.

Plasmonic hot electrons are very unique for catalysis. In recently, Halas's group published work on Science to illustrate the quantifying contributions of hot carriers and thermal effect in plasmonic photocatalysis, and plasmon-induced hot carriers of Cu–Ru were demonstrated to act predominant effects on NH_3 decomposition by reducing activation barrier of reaction.[31] Similar to metals, plasmon-induced hot carriers from nonmetallic WO_{3-x} is expected to play great roles on promoting catalytic reaction. For nonmetallic plasmonic NPs, the hot carriers generated on the surface can easily react with the absorbed substances, while, their surface vacancies are unstable in solvent. Aiming to stabilize the nonmetallic plasmonic photocatalysts, one strategy is to marry with semiconductors for constructing heterostructures, and photoelectrons injection from semiconductor increases free carrier density and keeps SPR of

Prof. Z. Z. Lou, Dr. J. Li, Dr. X. G. Yang, Prof. B. J. Li
Institute of Nanophotonics
Jinan University
Guangzhou 511443, China
E-mail: zzlou@jnu.edu.cn; baojunli@jnu.edu.cn
Dr. P. Zhang
Division of Environmental Science and Engineering
Pohang University of Science and Technology
Pohang 37673, Korea
Prof. B. B. Huang
State Key Laboratory of Crystal Materials
Shandong University
Jinan 250100, China
E-mail: bbhuang@sdu.edu.cn

DOI: 10.1002/adfm.201808696

nonmetallic NPs, which is preliminarily confirmed in our very recent work of CdS/WO_{3-x} nanowires with stable plasmonic hydrogen generation.[32] However, the construction of heterostructures with fast and continuous photoelectron injection is still one great challenge. Band structures, carrier migration ability, interface transfer, and electron storage capacity of semiconductors are all important for constructing stable nonmetallic plasmonic materials. TiO_2 is well known n-type semiconductor with high electron migration,[33] and WO_3 can store electrons as electrochromic materials.[34,35] Tungsten oxides with defects are reported as photocatalysts for CO_2 reduction,[36] while, the effect of their SPR on CO_2 reduction is unclear and it is necessary to be studied. The constructed TiO_2/WO_{3-x} heterostructure is expected not only as one stable nonmetallic plasmonic photocatalysts with continuous photoelectrons injection, but also as one potential strategy for efficient CO_2 photoreduction.

In this work, nonmetallic plasmonic WO_{3-x} nanowires (WO_{3-x}-NWs) were loaded on the mesoporous crystal structure TiO_2 (TiO_2-MCs), by one-step solvothermal process, and the heterostructures (TiO_2-MCs/WO_{3-x}-NWs) were obtained as plasmonic photocatalysts for hydrogen generation and CO_2 reduction. Photocatalytic results show that the hot electrons generation on WO_{3-x}-NWs have dominant role but low efficiency for hydrogen generation under visible light irradiation. When TiO_2-MCs/WO_{3-x}-NWs was used as co-catalyst free plasmonic photocatalyst for CO_2 reduction, and their activity for CH_4 generation (16.3 μmol g^{-1} h^{-1}) is fourfold and twofold higher than those of TiO_2-MCs (3.5 μmol g^{-1} h^{-1}) and WO_{3-x}-NWs (8.0 μmol g^{-1} h^{-1}) under solar light irradiation, respectively. Photoelectron injection of TiO_2-MCs was demonstrated by photoluminescence (PL) study to play a great role for stable SPR of WO_{3-x}, and plasmon-induced hot carrier leads to CH_4 generation with efficiency and high selectivity.

2. Results and Discussion

Tungsten oxides (WO_{3-x}) were synthesized by the simple one-step solvothermal procedure,[16] and the morphologies are nanowires with the diameter of 5 nm and the length of 20 nm aggregated to be bunches (**Figure 1**a and Figure S1, Supporting Information). Crystal structure of as-prepared WO_{3-x}-NWs belongs to that of $W_{18}O_{49}$ from X-ray diffraction (XRD) pattern (Figure S2, Supporting Information), and abundant W^{5+} and adsorbed oxygen species at the defect were detected by X-ray photoelectron spectroscopy (XPS) (Figure S2, Supporting Information), demonstrating the existence of oxygen vacancies in the crystal structure. TiO_2-MCs (Figure 1b,c) were fabricated by following the reported methods,[37] showing microsize plates and smooth surface. Selected area electron diffraction (SAED) (Figure S3, Supporting Information) demonstrated the single crystal structure of TiO_2-MCs. The heterostructures (Figure 1d,e) coupled with TiO_2-MCs and WO_{3-x}-NWs were synthesized by in situ growth of WO_{3-x}-NWs on TiO_2-MCs during solvothermal process. Surface of TiO_2-MCs becomes rough after WO_{3-x}-NWs loaded, which is observed clearly on the edges of microplates. From high resolution transmission electron microscopy (HRTEM) image of Figure 1f, the lattice spacing of 0.380 and 0.189 nm correspond to (010) planes of $W_{18}O_{49}$ and (200) planes of TiO_2, respectively, demonstrating the compositions

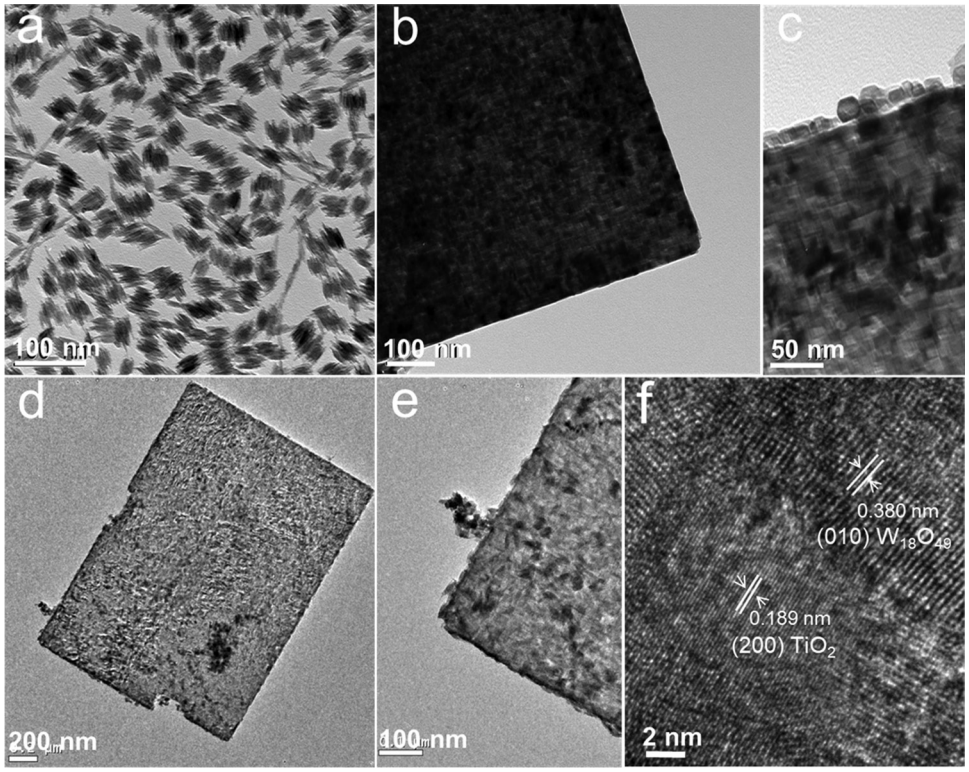

Figure 1. TEM images of WO_{3-x}-NWs a), TiO_2-MCs b,c), WO_{3-x}-NWs/TiO_2-MCs-2 d,e), and HRTEM image of WO_{3-x}-NWs/TiO_2-MCs-2 f).

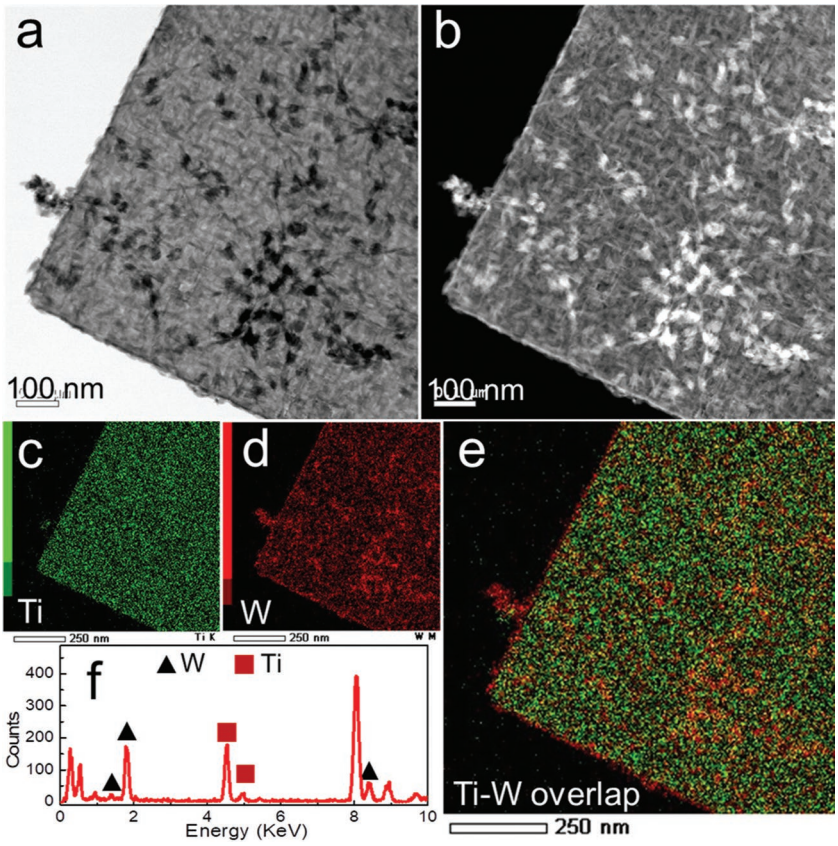

Figure 2. STEM a) and HAADF STEM b) of TiO_2-MCs/WO_{3-x}-NWs-2. Element mapping images Ti: c), W: d), Ti-W overlap: e), and EDX spectra f) of TiO_2-MCs /WO_{3-x}-NWs-2.

of heterostructures. XRD patterns and XPS spectrum further confirmed the crystal structure and composition in the heterostructures (Figure S4, Supporting Information). Moreover, the ratio between XPS bands of adsorbed oxygen species at the defect (532.2 eV)[38] and O–W (530.5 eV) in TiO_2/WO_{3-x} is larger than that in pure WO_{3-x}, indicating the more oxygen vacancies existence in the heterostructures. To analyze the structures of TiO_2-MCs/WO_{3-x}-NWs, measurements of scanning transmission electron microscope (STEM) and high-angle annular dark field STEM (HAADF-STEM) (**Figure 2**a,b) were done to clearly show that the growth of WO_{3-x} nanowires is along the surface of TiO_2-MCs and some bunches exist due to the aggregation. The existence and distribution of W and Ti elements are revealed by element mapping images (Figure 2c–e) and energy dispersive X-ray (EDX) spectra (Figure 2f). The molar ratio between WO_{3-x} and TiO_2 is calculated to be 1:10, and the sample is labeled as TiO_2-MCs/WO_{3-x}-NWs-2.

With abundant existence of oxygen vacancies in WO_{3-x} nanowires, the free charges density is high enough to occur in SPR, which has been demonstrated in theoretical modeling calculations.[39] From diffuse reflection spectroscopy (DRS) in **Figure 3**a, WO_{3-x} nanowires have a strong absorption from 400 nm to NIR region. While, TiO_2-MCs have only absorption in UV region. As-prepared TiO_2-MCs/WO_{3-x}-NWs-2 have a wide response region from UV–vis to NIR light, providing the possible to utilize of full-spectrum solar light. To test the photocatalytic performance of the heterostructure TiO_2-MCs/WO_{3-x}-NWs-2, 5 mg sample was mixed with 5 mL methanol (10 vol%) aqueous solution in 15 mL reaction chamber sealed with rubber stop. As shown in Figure 3b, little hydrogen is detected for TiO_2-MCs, attributing to its weak response to visible light. Plasmon-induced hot electrons from WO_{3-x} generated 27 μmol g^{-1} hydrogen in 30 min under visible light irradiation. In the heterostructures, TiO_2-MCs act as photoelectron injector to increase free carrier density and stabilize SPR of WO_{3-x}-NWs. Before photocatalytic reaction, TiO_2-MCs/WO_{3-x}-NWs-2 firstly irradiated under UV light for 30 min (preirradiation) to increase the electron density of WO_{3-x}. To keep same experiment sets, 30 min preirradiation was also done for TiO_2-MCs and WO_{3-x} before photocatalytic reaction. To our surprise, TiO_2-MCs/WO_{3-x}-NWs-2 generated 323 μmol g^{-1} hydrogen in 30 min under visible light irradiation, which is 11-fold higher than that of WO_{3-x}-NWs. Effect of UV preirradiation on plasmonic hydrogen generation was investigated by varying irradiation time, as shown in Figure S5 in the Supporting Information; generated hydrogen (at 30 min) was measured to be 175, 267, and 323 μmol g^{-1} over TiO_2-MCs/WO_{3-x}-NWs-2 with 10, 20, and 30 min preirradiation, respectively. It proves that the photoelectrons injection from TiO_2-MCs plays a great role on hydrogen generation of WO_{3-x}-NWs. Four recycle reactions over TiO_2-MCs/WO_{3-x}-NWs-2 with 10 min preirradiation is repeated with 176, 172, 171, and 180 μmol g^{-1} hydrogen generation in 30 min (Figure 3c), demonstrating their stable structure and activity in photocatalysis. Under visible light irradiation, the hydrogen generation rate is decreased as reaction time is prolonged (Figure 3d), which is attributed to the decreased free carriers density of WO_{3-x}-NWs during photocatalysis.

Photocatalytic activity of samples under UV–vis light irradiation were investigated as shown in **Figure 4**a. Compared with TiO_2-MCs and TiO_2-MCs/WO_{3-x}-NWs, WO_{3-x}-NWs show much weak efficiency for hydrogen generation. Within 30 min, 32 μmol hydrogen was generated over TiO_2-MCs, which is threefold higher than 10 μmol hydrogen over TiO_2-MCs/WO_{3-x}-NWs, indicating that the photoelectron injection decrease the activity of TiO_2-MCs for photocatalytic hydrogen generation. In order to investigate the photoelectron injection process, TiO_2-MCs/WO_{3-x}-NWs was kept in dark for overnight to decrease the free charge density in WO_{3-x}-NWs, and hydrogen generation was monitored under UV–vis light irradiation. The hydrogen generation (Figure 4b) is slow from 0 to 20 min and then becomes fast from 20 to 30 min, finally becomes stable after 30 min, proving the continuous photoelectron injection from TiO_2-MCs to WO_{3-x}-NWs. Consequently, the photoelectrons injected from TiO_2 to WO_{3-x} are used in low efficiency for photocatalytic hydrogen generation.

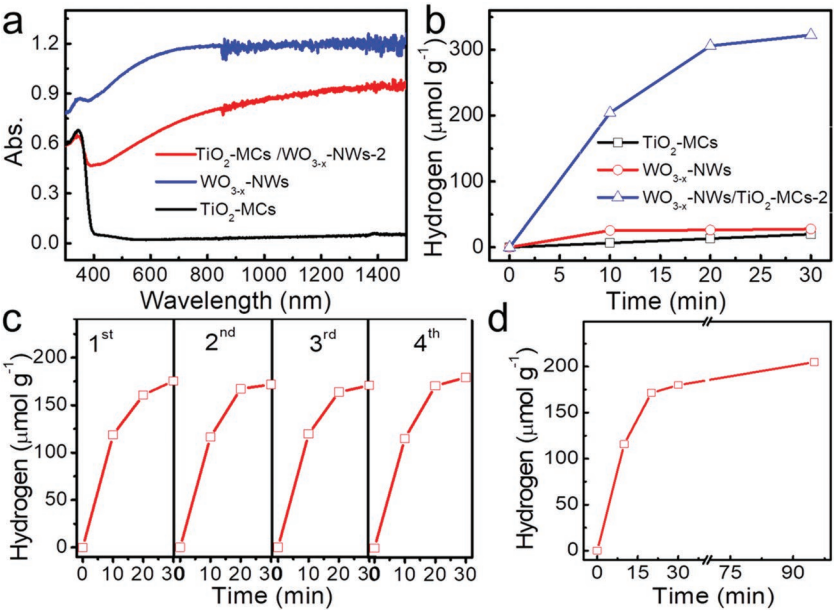

Figure 3. DRS a) of WO_{3-x}-NWs, TiO_2-MCs, and TiO_2-MCs/WO_{3-x}-NWs-2. Photocatalytic hydrogen generation b) over TiO_2-MCs, WO_{3-x}-NWs, and TiO_2-MCs/WO_{3-x}-NWs-2 as photocatalysts under visible light irradiation. Four times recycle reaction c) over TiO_2-MCs/WO_{3-x}-NWs-2 as photocatalysts with 10 min preirradiation. Photocatalytic hydrogen generation d) of TiO_2-MCs/WO_{3-x}-NWs-2 over reaction time. Co-catalyst: Pt (1 wt%). Light source: 200 W Xenon lamp (>420 nm).

The low hydrogen generation may, due to localized SPR of WO_{3-x} limiting the plasmon-induced hot carriers, transfer to non-uniform loaded co-catalyst Pt NPs on surface. To prove that injected photoelectrons have high efficiency for photocatalysis, CO_2 reduction over WO_{3-x} with co-catalyst free plasmonic photocatalysts was studied to evaluate the photocatalytic activity of TiO_2-MCs/WO_{3-x}-NWs. 5 mg TiO_2-MCs/WO_{3-x}-NWs-2 as photocatalysts was mixed with 0.2 mL water and plastered on cover glass (4.9 cm^2), and then sealed in 100 mL reaction chamber for CO_2 reduction. In 3 h, 49 μmol g^{-1} methane and 7.3 μmol g^{-1} carbon monoxide were generated over TiO_2-MCs/WO_{3-x}-NWs-2 as photocatalyst under UV–vis light irradiation, and to our surprise, no methanol was detected.(**Figure 5**a) Small amount of oxygen was detected during CO_2 photoreduction. Under visible light irradiation, only 2.0 μmol g^{-1} methane and 1.1 μmol g^{-1} carbon monoxide are generated, which are 24-fold and 6-fold lower than those generated over TiO_2-MCs/WO_{3-x}-NWs-2 under UV–vis light irradiation (Figure 5b). Under UV light irradiation, only 1.82 μmol g^{-1} methanol, 1.44 μmol g^{-1} carbon monoxides, and 1.25 μmol g^{-1} methane are generated as shown in Figure S6 in the Supporting Information. Without SPR, tungsten oxides exhibited no activity on photocatalytic CO_2 reduction.[36] Therefore, we conclude that the plasmon-induced hot carriers play predominant role on CO_2 reduction.

To support our conclusion, more experiment sets were done. Different compositions of TiO_2-MCs/WO_{3-x}-NWs were synthesized by varying the volumes of $W(CO)_6$ solution during solvothermal procedure. Three different samples labeled as TiO_2-MCs/WO_{3-x}-NWs-1, TiO_2-MCs/WO_{3-x}-NWs-2, and TiO_2-MCs/WO_{3-x}-NWs-3 were obtained as shown in scanning electron microscopy (SEM) images of Figure S7 in the Supporting Information, and their molar ratio between WO_{3-x} and TiO_2 was calculated by EDX spectra as 0.5:10, 1:10, and 2:10, respectively. Within 3 h, the product of methane was measured to be 38, 49, and 34 μmol g^{-1} for TiO_2-MCs/WO_{3-x}-NWs-1, TiO_2-MCs/WO_{3-x}-NWs-2, and TiO_2-MCs/WO_{3-x}-NWs-3, respectively.(**Figure 6**a) And carbon monoxide was detected to be 6.9, 7.3, and 6.3 μmol g^{-1} for TiO_2-MCs/WO_{3-x}-NWs-1, TiO_2-MCs/WO_{3-x}-NWs-2, and TiO_2-MCs/WO_{3-x}-NWs-3, respectively.(Figure 6b) On increasing of WO_{3-x}, more active sites and strong SPR are positive for CO_2 reduction. However, too much loading will reduce the UV light absorption of TiO_2 resulting in decreased photoelectrons injection. Consequently, TiO_2-MCs/WO_{3-x}-NWs-2 with strong SPR and photoelectron injection exhibited optimal activity (49 μmol g^{-1}, CH_4) for CO_2 reduction, which is fivefold high than that of TiO_2-MCs (10 μmol g^{-1}, CH_4). For pure WO_{3-x}-NWs, UV light irradiation excited electron transfer from valence band to conduct band, and the generated photoelectrons on conduct band increased carrier density and SPR, leading to higher photocatalytic activity (24 μmol g^{-1}, CH_4) of WO_{3-x}-NWs than TiO_2-MCs, but twofold lower than TiO_2-MCs/WO_{3-x}-NWs-2. Carbon monoxides and methanol is intermediate product of CO_2 reduction. TiO_2-MCs show highest activity than other samples in monoxide generation (at 3 h, 13 μmol g^{-1}, CO) and WO_{3-x} nanowires exhibited activity in methanol generation (at 3 h, 4.2 μmol g^{-1}, methanol). Generation rate and selectivity of products were calculated as shown in Figure 6c,d. For TiO_2-MCs, TiO_2-MCs/WO_{3-x}-NWs-1, TiO_2-MCs/WO_{3-x}-NWs-2, TiO_2-MCs/WO_{3-x}-NWs-3, and WO_{3-x}-NWs, their methane generation rate is 3.5, 12.7, 16.3,

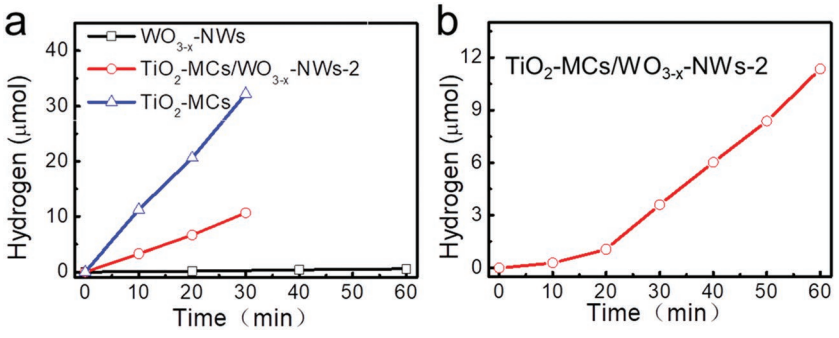

Figure 4. Hydrogen generation a) over WO_{3-x}-NWs, TiO_2-MC, and TiO_2-MCs/WO_{3-x}-NWs-2 as photocatalysts under UV–vis light irradiation. Hydrogen generation of TiO_2-MCs/WO_{3-x}-NWs-2 (kept in dark for one day before irradiation) over reaction time under UV–vis light irradiation b). Co-catalyst: Pt (1 wt%). Light source: 200 W Xenon lamp.

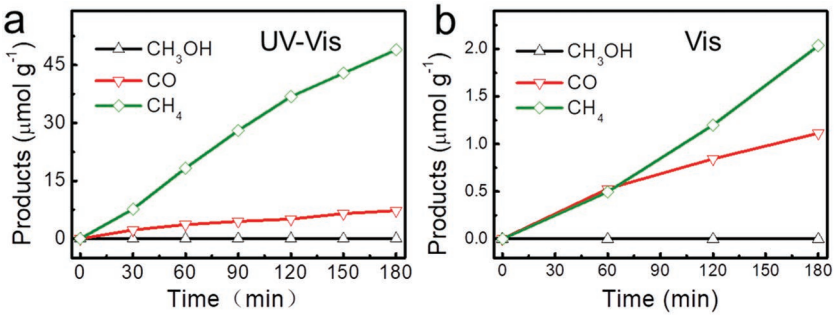

Figure 5. Products of CO_2 photoreduction over TiO_2-MCs/WO_{3-x}-NWs-2 as photocatalyst under UV–vis a) and visible b) light irradiation.

11.5, and 8.0 μmol g^{-1} h^{-1}, respectively, and their selectivity is calculated to be 42%, 80%, 83%, 81.7%, and 64%, respectively; While, their carbon monoxides generation rate is 3.7, 2.2, 2.4, 2.1, and 3.0 μmol g^{-1} h^{-1}, respectively, and their selectivity is 44%, 14.4%, 12.4%, 14.9%, and 23.7%, respectively. Furthermore, some C2 compounds (ethane and ethene) were detected (0.91 μmol g^{-1} h^{-1}) over TiO_2-MCs/WO_{3-x}-NWs-2 as photocatalysts. Only TiO_2-MCs and WO_{3-x}-NWs show generation of methanol with rate of 0.74 and 1.3 μmol g^{-1} h^{-1}, and their selectivity is 8.7% and 10%. Consequently, TiO_2-MCs/WO_{3-x}-NWs-2 has optimal compositions to exhibit high activity and selectivity in methane generation during CO_2 photoreduction.

The photoelectron transfer between TiO_2 and WO_{3-x} was investigated by the photoluminescence spectra which were measured by microspectrophotometer. With excitation of 365 nm light, two PL bands labeled as PL1 and PL2 are observed for pure TiO_2-MCs sample (**Figure 7**a). When combined with WO_{3-x}, the intensity of both PL1 and PL2 is decreased as shown in Figure 7b, and the quenching efficiency (Figure S8, Supporting Information) of PL1 and PL2 was calculated to be 22.5% and 30.6% for TiO_2-MCs/WO_{3-x}-NWs-1. No PL bands are observed from WO_{3-x}-NWs (Figure S9, Supporting Information) because their photoelectrons are trapped on the defects caused by the abundant oxygen vacancies. As the amount of WO_{3-x} increases, the quenching efficiency of PL1 and PL2 becomes 37.9% and 39.2% for TiO_2-MCs/WO_{3-x}-NWs-2, while, 40.7% and 42.5% for TiO_2-MCs/WO_{3-x}-NWs-2, respectively. PL quenching of TiO_2-MCs demonstrates the charge transfer between TiO_2-MCs and WO_{3-x}-NWs. Generation and transfer of photoelectrons in heterostructure was illustrated in the diagram (Figure 7c). Under UV light irradiation, electron on valence band (VB) of TiO_2 is excited and transfers to the conduct band (CB). The photoelectron on CB (E_{CB}) has a direct irradiative decay to recombine with hole on VB (E_{VB}) emitting one high energy photon as the PL1 band (around 450 nm). With the surface defect, photoelectron on CB (E_{CB}) transfers (CT_1) to surface defect energy level (E_S), and then recombines with hole on VB (E_{VB}) to emit one low energy photon as PL2 band (around 520 nm). For WO_{3-x}-NWs, abundant oxygen vacancies make free carriers on CB which occur in oscillation with incident light to exhibit SPR phenomenon. The free electrons occupy low energy level of CB, and electrons on VB are excited by short-wavelength light and transfer to the lowest vacant energy level (E_V) of CB, which limits UV light utilization. Under visible light irradiation, the free electrons on CB of WO_{3-x} are excited to be hot electron on high energy level which has more power to react with carbon dioxides. When the hot electrons are removed, free electron density is decreased resulting in weak SPR, and which leads WO_{3-x} to being weak SPR and low activity in plasmonic photocatalysis. In the obtained heterostructures, under UV–vis light irradiation, the excited photoelectrons on TiO_2 have charge transfer (CT_2 and CT_3) to WO_{3-x} which has been demonstrated by PL quenching study (Figure 7a,b). The continuous injection of photoelectrons stabilizes the free carriers density on CB of WO_{3-x}, meanwhile, the photoelectrons rapidly fill in the vacant energy level of CB after hot electrons are generated, leading to longer life time of the hot electrons to reduce carbon dioxides for methane and carbon monoxide generation under UV–vis light irradiation. Consequently, the synergetic effects of photoelectron injection of TiO_2-MCs and nonmetallic SPR of WO_{3-x}-NWs make heterostructure TiO_2-MCs/WO_{3-x}-NWs with high activity and selectivity on carbon dioxides photoreduction.

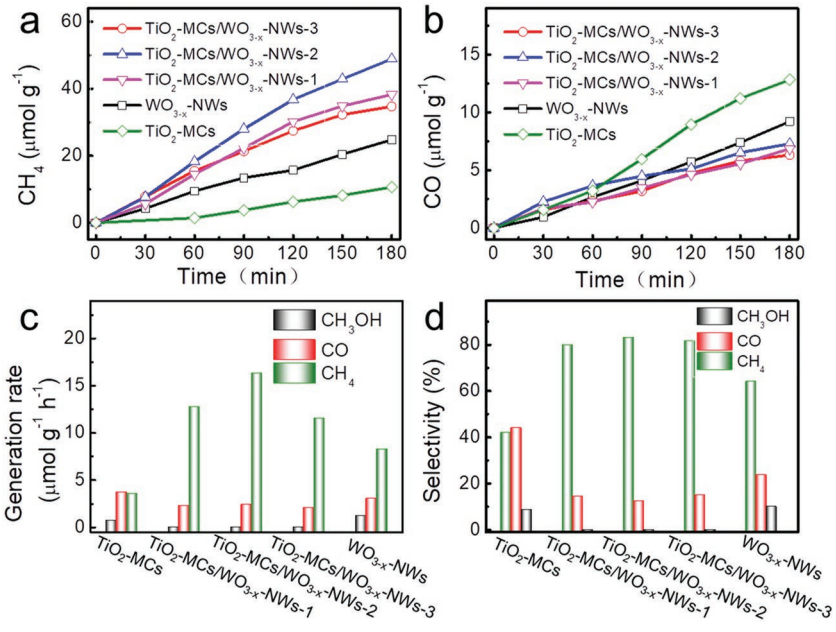

Figure 6. CH_4 a), CO b), and their generation rate c), and selectivity d) over different photocatalysts: TiO_2-MCs, TiO_2-MCs/WO_{3-x}-NWs-1, TiO_2-MCs/WO_{3-x}-NWs-2, TiO_2-MCs/WO_{3-x}-NWs-3, and WO_{3-x}-NWs under UV–vis light irradiation. Light source: 200W Xenon lamp.

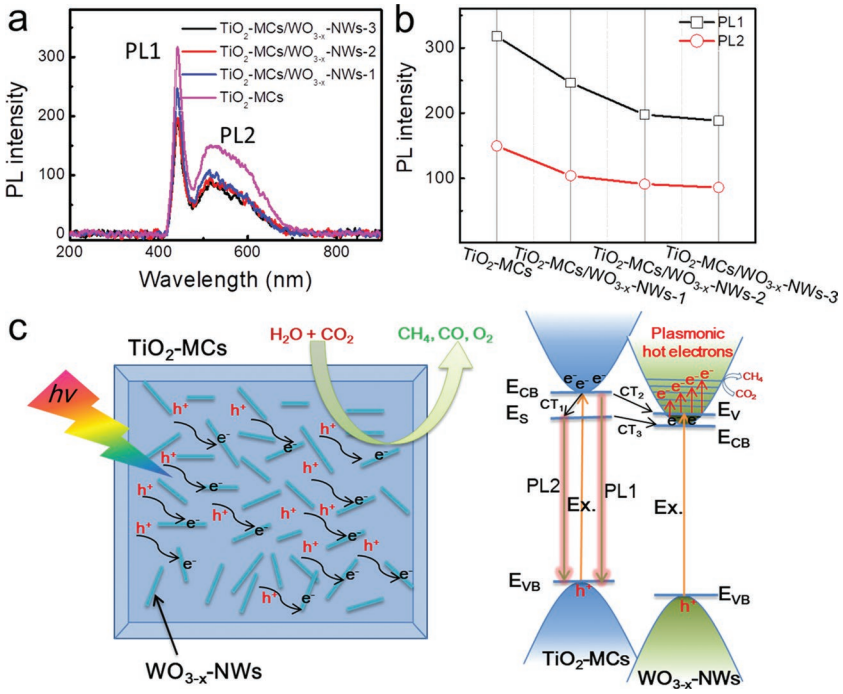

Figure 7. PL spectra a) and intensity b) of different samples: TiO_2-MCs, TiO_2-MCs/WO_{3-x}-NWs-1, TiO_2-MCs/WO_{3-x}-NWs-2, and TiO_2-MCs/WO_{3-x}-NWs-3. Excitation wavelength: 365 nm. Mechanism diagram c) of photoelectron generation and transfer in TiO_2-MCs/WO_{3-x}-NWs. E_{VB}: valence band; E_{CB}: conduct band; E_S: surface defect energy level; E_V: lowest vacant energy level on conduct band; CT_1: charge transfer of photoelectron from E_{CB} to E_S on TiO_2; CT_2: charge transfer of photoelectron from E_{CB} (TiO_2) to E_V (WO_{3-x}); CT_3: charge transfer of photoelectron from E_S (TiO_2) to E_V (WO_{3-x}).

3. Conclusion

In summary, to stabilize SPR of nonmetallic plasmonic WO_{3-x}, heterostructure TiO_2-MCs/WO_{3-x}-NWs were constructed by coupling mesoporous crystal TiO_2-MCs and nonmetallic plasmonic WO_{3-x} nanowires through one-step solvothermal procedure. Continuous photoelectron injection from TiO_2 to WO_{3-x} increases the free carrier density of WO_{3-x}, leading to stable SPR absorption and hot electron generation for plasmonic photocatalysis, which was demonstrated by the PL study. Photocatalytic results illustrate the dominant role of hot electrons of WO_{3-x} for hydrogen generation under visible light irradiation. Furthermore, TiO_2-MCs/WO_{3-x}-NWs with absence of noble metals as co-catalysts and SPR antenna are demonstrated to be highly active plasmonic photocatalysts for carbon dioxide reduction. The synergetic effects of photoelectron injection and nonmetallic SPR induced plasmonic hot electrons contributes to highly selective methane generation under UV–vis light irradiation.

4. Experimental Section

Materials: Titanium fluoride (TiF_4, >98.0%, Wako), ammonium nitrate (NH_4NO_3, >98%, Sigma-Aldrich), ammonium fluoride (NH_4F, >98.0%, Wako), tungsten hexacarbonyl ($W(CO)_6$, >97%, Sigma-Aldrich), ethanol (>99.5%), methanol (>99.5%), and carbon dioxides (>99.999%). All chemicals were used as purchased without any further purification.

Synthesis of TiO_2-MCs: MCs were prepared following the reported method. A mixed aqueous solution of TiF_4, NH_4NO_3, NH_4F, and ultrapure H_2O, with the molar ratio of 1:6.6:4:117 was dropped on a silicon wafer dropwise to form a thin layer. The precursor layer was annealed in air at 500 °C for 2 h with a ramping rate of 10 °C min^{-1}. The product was obtained after annealing at 500 °C in oxygen atmosphere for another 8 h to remove surface impurities.

Synthesis of TiO_2-MCs/WO_{3-x}-NWs: TiO_2-MCs/WO_{3-x}-NWs were synthesized by following the previous work.[16] In a typical procedure, 10 mg TiO_2-MCs were mixed with 30 mL ethanol, and then 2 mL $W(CO)_6$ solution (2 g L^{-1}) was added. Then, the solution was transferred to a 50 mL Teflon-lined stainless steel autoclave, and heated up to 160 °C for 12 h. The produced sample TiO_2-MCs/WO_{3-x}-NWs-1 was separated from the solution by centrifugation, washed with ethanol three times, and dried in a vacuum oven. The TiO_2-MCs/WO_{3-x}-NWs-2 and TiO_2-MCs/WO_{3-x}-NWs-3 were synthesized following the above same experiment set, with just the change of $W(CO)_6$ solution volumes with 4 and 6 mL, respectively, and the total solution volume kept as same.

Photocatalytic Hydrogen Generation: 5 mg TiO_2-MCs/WO_{3-x}-NWs were dispersed in 5 mL aqueous solution containing 10 vol% methanol using an ultrasonic bath, and then the mixture solution was sealed in 15 mL reaction chamber. Subsequently, the chamber was degassed with Argon for 30 min to completely remove the dissolved oxygen and it was ensured that the reactor was in an anaerobic condition. Then, the tube was irradiated under visible light (Asahi Spectra, LAX-C100) with magnetic stirring at room temperature. A 420 nm, cut-off filter was used to remove UV light. Hydrogen evolution was measured by using Shimadzu GC-2014A gas chromatograph with thermal conductivity detector (TCD).

Photocatalytic Carbon Dioxides Reduction: 5 mg TiO_2-MCs/WO_{3-x}-NWs was mixed with 0.2 mL pure water and plastered on cover glass (4.9 cm^2), which promises the same irradiation area. The cover glass coated samples were putt on bottom of reaction chamber (100 mL), and the side with samples coating was upside. The chamber was sealed with thick quartz cover glass and degassed with pure carbon dioxide gas for 20 min. The reaction was started under irradiation of UV–vis light (Perfectlight, PLS-SXE300D). The generation of methane, carbon monoxide, and methanol was measured by gas chromatography (Shimadzu, GC-2014A) with one TCD and two flame ionization detector (FID). Other reaction followed the same procedure under different light irradiation.

Characterizations: The samples were characterized using XRD (Rigaku Rint-2500, CuK source), SEM (JEOL JSM-6330FT), TEM (JEOL, 2100, operated at 100 KV), and high-resolution TEM (JEM-3000F, operated at 300 KV). UV–vis diffuse reflectance spectra were obtained on a JASO V-570 UV–vis/NIR spectrophotometer. XPS was performed with a JEOL JPS-9010 MC spectrometer. The adventitious carbon (C 1s located at 284.6 eV) was used as reference to binding energy. PL measurement was carried by using UV–vis microspectrophotometer (CRAIC TECHNOLOGIES, 20/30 PV) with 365 nm as excitation light.

Supporting Information

Supporting Information is available from the Wiley Online Library or from the author.

Acknowledgements

This work was supported by the National Natural Science Foundation of China (No. 51872125, 21703083, and 11804120), Guangdong Natural Science Funds for Distinguished Young Scholar (No. 2018B030306004), the Natural Science Foundation of Guangdong Province (2017A030310463) and the Project supported by GDUPS(2018).

Conflict of Interest

The authors declare no conflict of interest.

Keywords

artificial photosynthesis, carbon dioxide reduction, nonmetallic SPR, photocatalysis, plasmonic hot electron

Received: December 6, 2018
Revised: December 31, 2018
Published online:

[1] S. Y. Wang, Y. Y. Gao, S. Miao, T. F. Liu, L. C. Mu, R. G. Li, F. T. Fan, C. Li, *J. Am. Chem. Soc.* **2017**, *139*, 11771.
[2] Z. Z. Lou, S. Kim, M. Fujitsuka, X. G. Yang, B. J. Li, T. Majima, *Adv. Funct. Mater.* **2018**, *28*, 1706969.
[3] J. W. Hong, D. H. Wi, S. U. Lee, S. W. Han, *J. Am. Chem. Soc.* **2016**, *138*, 15766.
[4] P. Wang, B. B. Huang, X. Y. Qin, X. Y. Zhang, Y. Dai, J. Y. Wei, M. H. Whangbo, *Angew. Chem., Int. Ed.* **2008**, *47*, 7931.
[5] N. N. Jiang, X. L. Zhuo, J. F. Wang, *Chem. Rev.* **2018**, *118*, 3054.
[6] A. Manzi, T. Simon, C. Sonnleitner, M. Döblinger, R. Wyrwich, O. Stern, J. K. Stolarczyk, J. Feldmann, *J. Am. Chem. Soc.* **2015**, *137*, 14007.
[7] G. Kumari, X. Q. Zhang, D. Devasia, J. Heo, P. K. Jain, *ACS Nano* **2018**, *12*, 8330.
[8] S. J. Yu, A. J. Wilson, J. Heo, P. K. Jain, *Nano Lett.* **2018**, *18*, 2189.
[9] C. Clavero, *Nat. Photonics* **2014**, *8*, 95.
[10] T. Ding, J. Mertens, A. Lombardi, O. A. Scherman, J. J. Baumberg, *ACS Photonics* **2017**, *4*, 1453.
[11] Y. X. Wang, S. S. Wang, S. P. Zhang, O. A. Scherman, J. J. Baumberg, T. Ding, H. X. Xu, *Nano Res.* **2018**, *11*, 6384.
[12] G. Garcia, R. Buonsanti, E. L. Runnerstrom, R. J. Mendelsberg, A. Llordes, A. Anders, T. J. Richardson, D. J. Milliron, *Nano Lett.* **2011**, *11*, 4415.
[13] R. Buonsanti, A. Llordes, S. Aloni, B. A. Helms, D. J. Milliron, *Nano Lett.* **2011**, *11*, 4706.
[14] J. M. Luther, P. K. Jain, T. Ewers, A. P. Alivisatos, *Nat. Mater.* **2011**, *10*, 361.
[15] M. Kanehara, H. Koike, T. Yoshinaga, T. Teranishi, *J. Am. Chem. Soc.* **2009**, *131*, 17736.
[16] Z. Z. Lou, Q. Gu, L. Xu, Y. S. Liao, C. Xue, *Chem. - Asian J.* **2015**, *10*, 1291.
[17] Z. Z. Lou, Q. Gu, Y. S. Liao, S. J. Yu, C. Xue, *Appl. Catal., B* **2016**, *184*, 258.
[18] S. Ishii, S. L. Shinde, T. Nagao, *Adv. Opt. Mater.* **2018**, *7*, 1800603.
[19] Y. Kuwahara, Y. Yoshimura, K. Haematsu, H. Yamashita, *J. Am. Chem. Soc.* **2018**, *140*, 9203.
[20] H. F. Cheng, M. C. Wen, X. C. Ma, Y. Kuwahara, K. Mori, Y. Dai, B. B. Huang, H. Yamashita, *J. Am. Chem. Soc.* **2016**, *138*, 9316.
[21] X. L. Wang, Y. J. Ke, H. Y. Pan, K. Ma, Q. Q. Xiao, D. Q. Yin, G. Wu, M. T. Swihart, *ACS Catal.* **2015**, *5*, 2534.
[22] R. Alam, M. Labine, C. J. Karwacki, P. V. Kamat, *ACS Nano* **2016**, *10*, 2880.
[23] Z. F. Huang, J. J. Song, L. Pan, X. W. Zhang, L. Wang, J. J. Zou, *Adv. Mater.* **2015**, *27*, 5309.
[24] H. Zhu, Y. Wang, C. Chen, M. R. Ma, J. F. Zeng, S. Z. Li, Y. S. Xia, M. Y. Gao, *ACS Nano* **2017**, *11*, 8273.
[25] L. Wen, L. Chen, S. M. Zheng, J. F. Zeng, G. X. Duan, Y. Wang, G. L. Wang, Z. F. Chai, Z. Li, M. Y. Gao, *Adv. Mater.* **2016**, *28*, 5072.
[26] M. Yan, G. L. Li, C. S. Guo, W. Guo, D. D. Ding, S. H. Zhang, S. Q. Liu, *Nanoscale* **2016**, *8*, 17828.
[27] K. P. Yuan, Q. Cao, H. L. Lu, M. Zhong, X. Z. Zheng, H. Y. Chen, T. Wang, J. J. Delaunay, W. Luo, L. W. Zhang, Y. Y. Wang, Y. H. Deng, S. J. Ding, D. W. Zhang, *J. Mater. Chem. A* **2017**, *5*, 14697.
[28] H. F. Cheng, T. Kamegawa, K. Mori, H. Yamashita, *Angew. Chem., Int. Ed.* **2014**, *53*, 2910.
[29] Z. Y. Zhang, X. Y. Jiang, B. K. Liu, L. J. Guo, N. Lu, L. Wang, J. D. Huang, K. C. Liu, B. Dong, *Adv. Mater.* **2018**, *30*, 170522.
[30] Z. Y. Zhang, Y. Liu, Y. R. Fang, B. S. Cao, J. D. Huang, K. C. Liu, B. Dong, *Adv. Sci.* **2018**, *5*, 1800748.
[31] L. N. Zhou, D. F. Swearer, C. Zhang, H. Robatjazi, H. Q. Zhao, L. Henderson, L. L. Dong, P. Christopher, E. A. Carter, P. Nordlander, N. J. Halas, *Science* **2018**, *362*, 69.
[32] Z. Z. Lou, M. S. Zhu, X. G. Yang, Y. Zhang, M. H. Whangbo, B. J. Li, B. B. Huang, *Appl. Catal., B* **2018**, *226*, 10.
[33] M. L. Sushko, K. M. Rosso, J. Liu, *J. Phys. Chem. C* **2010**, *114*, 20277.
[34] N. E. Mendieta-Reyes, A. K. Diaz-Garcia, R. Gomez, *ACS Catal.* **2018**, *8*, 1903.
[35] H. X. Gu, C. S. Guo, S. H. Zhang, L. H. Bi, T. C. Li, T. D. Sun, S. Q. Liu, *ACS Nano* **2018**, *12*, 559.
[36] G. C. Xi, S. X. Ouyang, P. Li, J. H. Ye, Q. Ma, N. Su, H. Bai, C. Wang, *Angew. Chem.* **2012**, *124*, 2445.
[37] O. Elbanna, M. Fujitsuka, T. Majima, *ACS Appl. Mater. Interfaces* **2017**, *9*, 34844.
[38] N. Zhang, A. Jalil, D. X. Wu, S. M. Chen, Y. F. Liu, C. Gao, W. Ye, Z. M. Qi, H. X. Ju, C. M. Wang, X. J. Wu, L. Song, J. F. Zhu, Y. J. Xiong, *J. Am. Chem. Soc.* **2018**, *140*, 9434.
[39] K. Manthiram, A. P. Alivisatos, *J. Am. Chem. Soc.* **2012**, *134*, 3995.

